Design Procedure of Flux Reversal Permanent Magnet Machines

Yuting Gao, *Student Member, IEEE*, Ronghai Qu, *Senior Member, IEEE*, Dawei Li, *Member, IEEE*, Jian Li, *Member, IEEE*.

***Abstract*—Flux reversal permanent magnet machines (FRPMMs) exhibit many advantages such as simple rotor configuration, high torque density, fast transient response, etc. However, the general analytical design procedure of FRPMMs has not been established. Thus, this paper mainly focuses on developing an analytical design methodology of three-phase FRPMMs. First, the sizing equations are derived based on a magneto motive force (MMF)-permeance model. Then, the influences of several key parameters in the sizing equation including slot-pole combination, airgap radius, electric loading and equivalent magnetic loading on the torque density are analyzed. Moreover, the feasible slot-pole combinations are summarized and the corresponding winding type of each combination is recommended in order to maximize the output torque. Besides, the detailed geometric design of stator and rotor are presented. Finally, the proposed analytical design procedure is verified by finite element analysis (FEA) and experiments on a 12-stator-slot/17-rotor-slot FRPMM prototype.**

***Index Terms*-- Design procedure, flux reversal permanent magnet machine (FRPMM), sizing equation, finite element analysis (FEA).**

I. Introduction

FLUX REVERSAL permanent magnet machine (FRPMM) was first introduced in 1997 with the purpose of combining the advantages of switched reluctance machine (SRM) with robust rotor structure and permanent magnet (PM) machine with large torque density [1]. It exhibits many superior performances including simple construction, high fault tolerance, easy maintenance and fast transient response [2], [3]. Thus, FRPMM has been widely used in many applications such as electric vehicle propulsion [4], [5], low-speed servo systems [6] and direct-drive winding power generation [7]. Many researchers have done excellent work on the design and analyses of FRPMMs. First, for comparisons of FRPMM to other machine types, authors in [8] compared a FRPMM with a conventional fractional-slot concentrated-winding (FSCW) PM machine under the same geometric dimensions, electric loading and magnetic loading. It was

Manuscript received October 14, 2016. This work was supported by National Natural Science Foundation of China (NSFC) under Project Number 51520105010.

The authors are with the State Key Laboratory of Advanced Electromagnetic Engineering and Technology, School of Electrical and Electronic Engineering, Huazhong University of Science and Technology, Wuhan 430074, China (e-mail: daweili@hust.edu.cn).

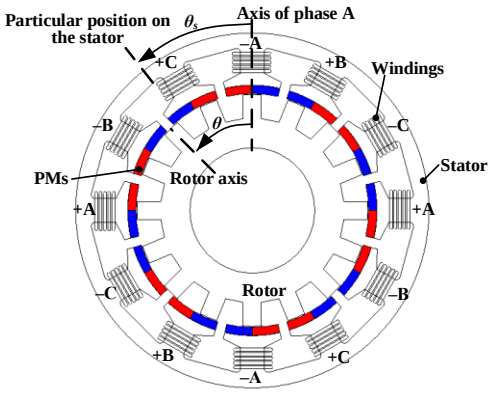

Fig. 1. Cross section of a FRPMM.

claimed that the FRPMM has a larger power density but a lower power factor than the FSCW PM machine. Also, qualitative comparisons have been made between the FRPMM and some other brushless machines including doubly-salient PM machine (DSPMM), SRM, and brushless dc machine in terms of operation principle, inductance, torque capabilities, etc. [1]. Moreover, as stator-PM machines, performances of FRPMM, DSPMM and flux switching PM machine (FSPMM) have also been evaluated together in [9]. Then, for torque density improvement of FRPMMs, many new FRPMM topologies have been presented such as consequent-pole FRPMM [10], FRPMMs with separate PM excitation stators [11]-[14], etc. Besides, by utilizing full-pitch windings which have a higher winding factor, the power density and efficiency of FRPMM can be increased as well [15]. However, owing to the doubly slotted structure, some FRPMMs suffer from big cogging torque, which not only produces undesired vibrations and noises, but also deteriorates machine performances. Hence, the reduction of cogging torque is of great importance and it has been managed by skewing [16], rotor teeth pairing [17], rotor pole shaping [18], dummy slot [19], asymmetrical rotor teeth [20], etc. In addition, many efforts have been made on the investigation of operation principles of FRPMM. It was found that the FRPMM can be regarded as a conventional PM machine coupled with a fictitious gear [21]-[23]. In other words, the FRPMM has a similar torque production mechanism with the magnetic geared machine or vernier machine [24]-[27]. For the design issue of FRPMMs, the formulae for geometrical parameter calculations are presented based on the classic design method in [28]. Then, the effects of structural dimensions on average torque [3] and pulsating torque are analyzed in [29] with the employment of several

analytical equations. And authors in [30] introduces a design of a FRPMM using time-stepping finite element analysis (FEA). However, in most of those papers, the specific design of FRPMMs are mainly based on the classical design method [28], or FEA [10]-[20], [30], or the analytical method that cannot be directly applied and obviously show the influences of key parameters on torque [3], [29]. Therefore, in this paper, the specialized sizing equations for FRPMMs will be derived and the analytical design procedure will be developed, which can be directly employed in the initial design of FRPMMs and allows for fast calculations of machine dimensions.

This paper is organized as follows. First, the structure and operation principles are introduced. Then in Section III, the sizing equations are analytically derived and the influences of several key parameters (slot-pole combination, airgap radius, electric loading and equivalent magnetic loading) in the sizing equation on the torque density are analyzed. Also, the effects of the airgap structural parameters on the power factor are investigated. Moreover, in Section IV, the geometric design of stator and rotor are introduced. And in Section V, the design procedure is illustrated. Besides, in order to check the validity of the proposed analytical design method, a case study is presented and a FRPMM prototype is tested. Finally, conclusions are drawn in Section VI.

II. Structure and Operation Principle

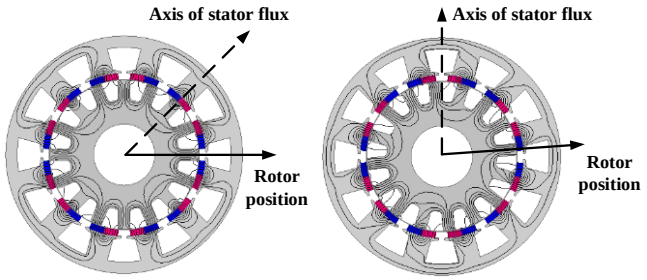

Fig. 2. Flux distributions of the 12-stator-slot/16-rotor-slot FRPMM: (a) Rotor position at 0 degree; (b) Rotor position at 5.625 degree (1/4 rotor slot pitch).

The cross-section of a FRPMM is shown in Fig. 1. The FRPMM is composed of a simple reluctance rotor and a stator with a pair of PMs attached to the teeth surface. The slot-pole combination of three-phase FRPMMs are ruled by the following equation [31]:

$$P = \min\left\{ P = \frac{iZ_s}{2} \pm Z_r; \quad \frac{Z_s}{GCD(Z_s, P)} = 3k \right\} \tag{1}$$

$$i = 1,3,5... \qquad k = 1,2,3...$$

where P is the winding pole pair, Z_s and Z_r are the number of stator and rotor slots, respectively. Therefore, the feasible slot-pole combinations can be summarized as Table I. In this table, *SPP* stands for slot per pole per phase and *PR* equals the ratio of Z_r to P. Non-overlapping windings are frequently employed in FRPMMs due to their fault tolerance capability and easy manufacture, while some slot-pole combinations of FRPMMs are recommended to adopt overlapping windings to achieve a higher winding factor. Hence, the winding factors k_{wn} and k_{wr} are calculated based on non-overlapping windings and recommended winding types, respectively. To explicate the operating principle, a FRPMM with 2 pole-pair windings, 12 stator slots and 16 rotor slots is taken as an instance. The flux distributions with different rotor positions are shown in Fig. 2. The magnetic field is generated only by the magnets, and the difference of the rotor positions corresponds to 5.625 mechanical degrees (i.e. 1/4 rotor slot pitch). It can be observed that pole pair number of stator magnetic field is 2. Thus, a 2 pole-pair back-EMF can be yielded, and then the steady torque will be produced by the interaction between the 2 pole-pair back-EMF and the 2 pole-pair armature field. Moreover, it can be seen that the axis of stator flux rotates by 45 degrees due to the change of rotor position (5.625 degrees). In other words, the small rotor position displacement results in a large variation of stator flux distribution, which would introduce the vernier effect to FRPMMs. Besides, the ratio of the displacement between the rotor position and the stator flux equals the pole ratio (*PR*), which is 8 in the 12-stator-slot/16-rotor-slot FRPMM. In addition, it should be noted that the rotating directions of rotor and stator fields are opposite, thus the stator currents i_a, i_b, i_c should be in negative phase sequence.

III. Sizing Equation of FRPMM

A. Torque Equation

The torque equation can be analytically derived through the analysis of the magnet MMF and airgap permeance function. In order to simplify the analysis, the following assumptions should be made beforehand:

- The magnetic resistance of the iron part is neglected.
- The airgap flux density only varies along the circumferential direction and does not change along the radial direction.
- The FRPMM is supplied by symmetrical sinusoidal three-phase currents.

First, the definitions of several mechanical angles are illustrated in Fig. 1. The magnetic motive force (MMF) developed by the magnets can be expressed as [31]:

$$F(\theta_s) \approx F_1 \sin\left(\frac{Z_s}{2}\theta_s\right) + F_3 \sin\left(\frac{3Z_s}{2}\theta_s\right) \tag{2}$$

where F_1 and F_3 are the magnitudes of fundamental and 3rd harmonic respectively. They can be given as:

$$F_1 = \frac{4}{\pi}\frac{B_r h_m}{\mu_r \mu_0}\left(1 - \sin\frac{\pi\alpha_{so}}{2}\right) \tag{3}$$

$$F_3 = \frac{4}{3\pi}\frac{B_r h_m}{\mu_r \mu_0}\left(1 + \sin\frac{3\pi\alpha_{so}}{2}\right) \tag{4}$$

where B_r, μ_r and h_m are the remanent flux density, relative permeability and thickness of the magnets, respectively, α_{so} is the slot opening ratio which equals the ratio of slot opening width to slot pitch. Then, the airgap flux density can be derived based on MMF-permeance model:

TABLE I
SLOT-POLE COMBINATIONS OF THREE-PHASE FRPMM

Z_s	Z_r	2	3	4	5	6	7	8	10	11	12	13	14	15	16	17	19	20
6	P	1		1	2		2	1	1	2		2	1		1	2	2	1
	SPP	1		1	0.5		0.5	1	1	0.5		0.5	1		1	0.5	0.5	1
	PR	2		4	2.5		3.5	8	10	5.5		6.5	14		16	8.5	9.5	20
	k_{wn}	0.5		0.5	0.866		0.866	0.5	0.5	0.866		0.866	0.5		0.5	0.866	0.866	0.5
	k_{wr}	1		1	0.866		0.866	1	1	0.866		0.866	1		1	0.866	0.866	1
12	P	4		2	1		1	2	4	5		5	4		2	1	1	2
	SPP	0.5		1	2		2	1	0.5	0.4		0.4	0.5		1	2	2	1
	PR	0.5		2	5		7	4	2.5	2.2		2.6	3.5		8	17	19	10
	k_{wn}	0.866		0.5	0.25		0.25	0.5	0.866	0.933		0.933	0.866		0.5	0.25	0.25	0.5
	k_{wr}	0.866		1	0.966		0.966	1	0.866	0.933		0.933	0.866		1	0.966	0.966	1
18	P	7	6	5	4	3	2	1	1	2	3	4	5	6	7	8	8	7
	SPP	3/7	0.5	0.6	0.75	1	1.5	3	3	1.5	1	0.75	0.6	0.5	3/7	0.375	0.375	3/7
	PR	2/7	0.5	0.8	1.25	2	3.5	8	10	5.5	4	3.25	2.8	2.5	16/7	2.13	2.38	20/7
	k_{wn}	0.902	0.866	0.735	0.617	0.5	0.492	0.167	0.167	0.492	0.5	0.617	0.735	0.866	0.902	0.945	0.945	0.902
	k_{wr}	0.902	0.866	0.945	0.945	1	0.945	0.96	0.96	0.945	1	0.945	0.945	0.866	0.902	0.945	0.945	0.902

PS: Non-overlapping windings are recommended. Others: Overlapping windings are recommended.
k_{wn} and k_{wr} are fundamental winding factor calculated based on non-overlapping winding type and recommended winding types, respectively.

$$B(\theta_s,\theta)=F_{PM}(\theta_s)P_g(\theta_s,\theta) \tag{5}$$

where $P_g(\theta_s,\theta)$ is the not the airgap permeance function but the rotor permeance function. Since the saliency of stator has been considered in Eqn. 2, the doubly-salient structure of FRPMM could be viewed as a unilateral salient structure on the rotor. The rotor permeance function is given as:

$$P_g(\theta_s,\theta)=P_0+P_1\cos\left\{Z_r\left(\theta_s-\theta\right)\right\} \tag{6}$$

The coefficients P_0 and P_1 can be worked out using the analytical approach proposed in [32]. Hence, the airgap flux density $B(\theta_s,\theta)$ could be rewritten as:

$$\begin{aligned}B(\theta_s,\theta)\approx{}&B_1\sin\left\{\left(Z_s/2-Z_r\right)\theta_s+Z_r\theta\right\}\\&+B_3\sin\left\{\left(3Z_s/2-Z_r\right)\theta_s+Z_r\theta\right\}\end{aligned} \tag{7}$$

where B_1=1/2F_1P_1, B_3=1/2F_3P_1. It can be found that the pole pair number of the fundamental and third harmonics are different, i.e. Z_s/2-Z_r and 3Z_s/2-Z_r, respectively. But the absolute values of the speed for fundamental and third harmonics in Eqn. 7 are identical, i.e.

$$\frac{d(Z_r\theta)}{dt}=Z_r\omega_m \tag{8}$$

where ω_m is the mechanical angular speed of rotor. Thus, both the two harmonics will contribute to the production of back-EMF, whose frequency can be derived as $Z_r\omega_m/2\pi$. It is known that a steady-state torque can be achieved only when the frequency and pole pair of the back-EMF are the same with that of the winding MMF respectively. Therefore, if the frequency of phase current is set as $Z_r\omega_m/2\pi$ (i.e. the rotation speed of winding MMF is synchronized with that of the airgap flux density) and the armature windings are wounded into P pole pairs, where P equals Z_s/2-Z_r or 3Z_s/2-Z_r, a steady-state torque can be obtained. Then, the no-load phase flux linkage can be expressed as:

$$\lambda_{ph}(\theta)=r_g l_{stk}\int_0^{2\pi}B(\theta_s,\theta)\sum_{j=1,3...}\frac{2}{j\pi}\frac{N_s}{P}k_{wj}\cos\left(jP\theta_s\right)d\theta_s \tag{9}$$

where r_g is airgap radius, l_{stk} is active stack length, N_s is the number of series turns per phase, and k_{wj} is the winding factor of the jth harmonics. It should be noted that as the order of B_1 and B_3 in Eqn. 7 are (Z_s/2-Z_r)/P and (3Z_s/2-Z_r)/P, respectively, they are tooth harmonics of each other, i.e. they have the same absolute values of winding factors in Eqn. 9 [29]. Then the back-EMF can be obtained as the derivative of the phase flux linkage:

$$\begin{aligned}E_{ph}(\theta)&=\frac{d}{dt}\lambda_{ph}(\theta)\\&=2N_s r_g l_{stk}\omega_m k_w Z_r\left\{\frac{B_1}{\left(\frac{Z_s}{2}-Z_r\right)\Big/P}\pm\frac{B_3}{\left(\frac{3Z_s}{2}-Z_r\right)\Big/P}\right\}\end{aligned} \tag{10}$$

where k_w is the winding factor of $\{(Z_s/2\text{-}Z_r)/P\}^{\text{th}}$ harmonic, and the upper positive convention is for the condition when the winding factor of $\{(3Z_s/2\text{-}Z_r)/P\}^{\text{th}}$ harmonic equals that of the $\{(Z_s/2\text{-}Z_r)/P\}^{\text{th}}$ harmonic, and the lower negative convention is for the condition when the two winding factors are opposite. Since the reluctance torque of FRPMM is negligible, the electromagnetic torque under i_d=0 control can be expressed as:

$$T_e=3I_p N_s r_g l_{stk}k_w Z_r\left\{\frac{B_1}{\left(\frac{Z_s}{2}-Z_r\right)\Big/P}\pm\frac{B_3}{\left(\frac{3Z_s}{2}-Z_r\right)\Big/P}\right\} \tag{11}$$

where I_p is the peak value of phase current. It can be seen in Eqn. 11 that T_e is proportional to pole ratio PR (=Z_r/P), i.e. the torque production mechanism of FRPMM is similar to that of vernier or magnetic geared machines. However, a larger PR does not always result in a higher average torque because T_e is also inversely proportional to (Z_s/2-Z_r)/P and (3Z_s/2-Z_r)/P, which are greatly affected by PR. Although the general torque equation has been achieved as Eqn. 11, significant design parameters such as electric loading, mechanical loading have not been reflected in the torque expression. Hence it is desirable to break Eqn. 11 to several basic factors which can be directly applied in the initial design stage.

The electric loading can be given as:

$$A_e=\frac{6N_sI_p}{2\sqrt{2}\pi r_g} \tag{12}$$

Then, the equivalent magnetic loading of three-phase FRPMM B_m is defined as:

$$B_m = \frac{B_1}{\left(\frac{Z_s}{2} - Z_r\right)\Big/P} \pm \frac{B_3}{\left(\frac{3Z_s}{2} - Z_r\right)\Big/P} \tag{13}$$

So, the torque expression in Eqn. 11 can be rewritten as:

$$T_e = \sqrt{2}\pi r_g^2 l_{stk} k_w Z_r A_e B_m \tag{14}$$

Thus, the rotor volume V_r, which equals $\pi l_{stk} r_g^2$, can be obtained:

$$V_r = \frac{T_e}{\sqrt{2} k_w Z_r A_e B_m} \tag{15}$$

and then the airgap radius r_g and the stack length l_{stk} can be derived as:

$$r_g = \sqrt[3]{V_r / (\pi k_{lr})} \tag{16}$$

$$l_{stk} = \sqrt[3]{V_r k_{lr}^2 / \pi} \tag{17}$$

where k_{lr} is the ratio of airgap radius r_g to stack length l_{stk}.

It can be found in Eqn. 14 that the key parameters affecting the torque density are airgap radius r_g, slot-pole combinations, electric loading A_e and equivalent magnetic loading B_m, which should be determined at the initial stage of the design process. Thus, the influences of the above key parameters on average torque will be investigated as the following part.

B. *Influence of Slot-Pole Combinations on Torque*

Fig. 3 investigates the effect of stator and rotor slot number combinations on the torque density when non-overlapping winding type and recommended winding type are employed, respectively. The detailed parameters of the models are listed in Table II. Since the airgap radius r_g and electric loading A_e are kept constant for these models, the main parameters affecting the output torque are winding factor k_w, pole ratio PR and equivalent magnetic loading B_m. It can be seen in Fig. 3(a) that the torque initially increases with Z_r as a result of a larger $PR*k_w$, and then it decreases since the flux modulation effect and B_m are reduced with more rotor slots. When the stator slot number are 6, 12 and 18, the optimal rotor slot number for maximal torque of FRPMMs with non-overlapping windings are 8, 14 and 21, respectively. However, in Fig. 3(b), when recommended windings are adopted, the optimal rotor slot number are 6, 17 and 10, respectively. As the winding factors k_w approximate to 1, the output torque are mainly influenced by PR and B_m. Since PR varies more dramatically than B_m under the given machine dimensions, the change trend of the average torque in Fig. 3(b) resembles that of PR in Table II. Moreover, it should be noted that the variation trends of the torque-Z_r curves with different stator slots are similar, while the curve moves rightwards as the stator slot number Z_s increases.

TABLE II
PARAMETERS OF THE FRPMM MODELS

Parameter	Value	Parameter	Value
Stator outer diameter	170mm	Stack length	100mm
Stator inner diameter	105m	Airgap length	0.5mm
Stator slot opening ratio	0.25	PM thickness	2.5mm
Rotor slot opening ratio	0.65	Magnet remanence	1.21T
Series turns per phase	80	Rated current	5.3A
Rated speed	600rpm	Remanent permeability	1.065

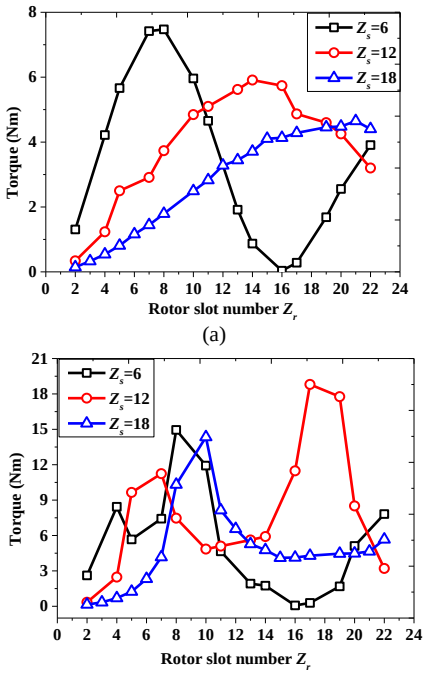

Fig. 3. Effect of stator and rotor slot combinations on torque: (a) non-overlapping windings; (b) recommended windings.

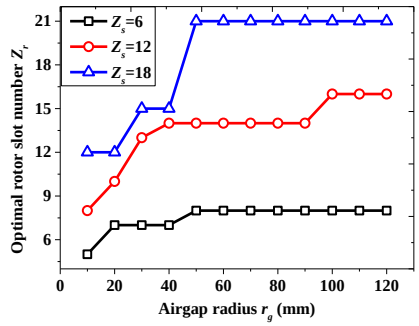

Fig. 4. Effect of airgap radius r_g on optimal rotor slot number when split ratio is 0.6.

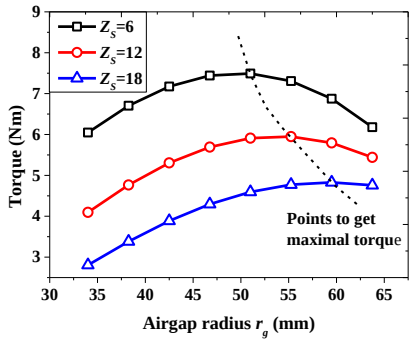

Fig. 5. Effect of airgap radius r_g on torque when stator outer diameter is 170mm.

C. *Influence of Airgap Radius on Torque*

Fig. 4 focuses on the effect of the airgap radius r_g on optimal Z_r at 6, 12 and 18 stator slots, respectively. It can be seen that when r_g is small, the optimized rotor slot number is low due to the large pole leakage flux. However, when r_g increases, the optimal Z_r rises as a result of the reduced leakage flux. Moreover, the influences of airgap radius on output torque are investigated in Fig. 5. It should be noted that when increasing r_g,

the stator outer diameter keeps constant, and the output torque is calculated with the optimal slot-pole combinations at different airgap radius r_g. It can be found that with the increase of airgap radius, the torque increases in the beginning, and it decreases afterwards. This is because when the airgap radius initially gets bigger, the rotor tooth width becomes larger and the flux modulation effect of the rotor teeth gets stronger. But when the airgap radius becomes bigger and bigger, the slot area dramatically decreases and the winding turns per phase is reduced. So the output torque goes down. Moreover, it can be seen that the points to get maximal torque move rightwards as the stator slot number increases. This is because the bigger the stator slot number, the larger the winding pole pair number and the less saturated the stator iron. Hence the optimal airgap radius increases with the stator slot number.

D. Influence of Magnetic Loading and Equivalent Electrical Loading on Torque

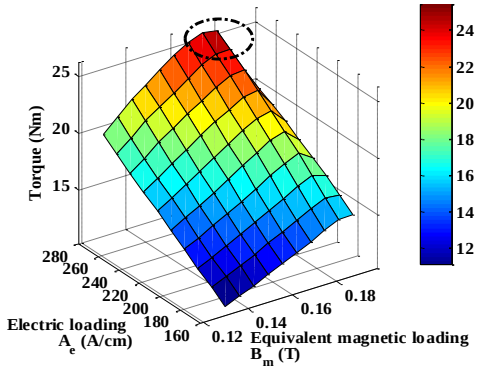

(a)

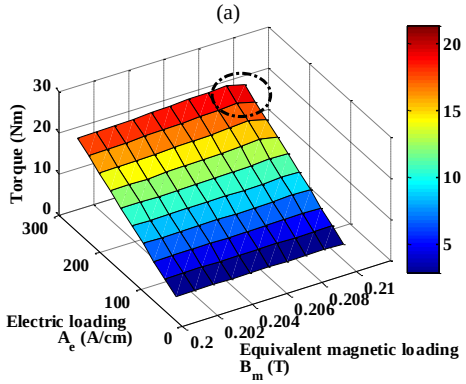

(b)

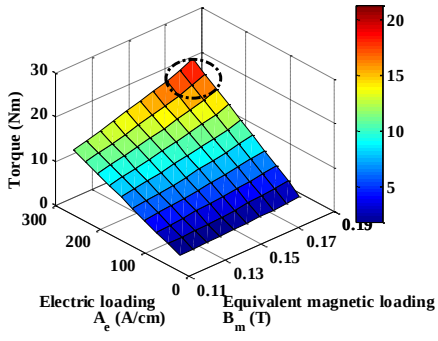

(c)

Fig. 6. Effect of equivalent magnetic loading and electric loading on torque: (a) Z_s=6; (b) Z_s =12; (c) Z_s =18.

The influences of equivalent magnetic loading B_m and electrical loading A_e on the output torque are shown in Fig. 6. The 6-, 12- and 18-stator-slot FRMs with r_g=55mm and the corresponding optimal rotor slot number are selected as representatives. Moreover, it should be noted that non-overlapping windings are adopted in the analyses because they are frequently used in literatures. One can find that when the electrical loading A_e is low, the average torque increases continuously with the equivalent magnetic loading because T_e is proportional to the product of A_e and B_m. However, as can be seen in Fig. 6 (a) and (b), when A_e becomes bigger and bigger, there is an optimal B_m for a maximal torque due to the saturation effect of stator and rotor iron. But in Fig. 6(c), the output torque monotonically increases with A_e and B_m. Since the winding pole pair of the 18-stator-slot FRPMM (i.e. 6) is larger than that of the 6-stator-slot FRPMM (i.e. 1) and 12-stator-slot FRPMM (i.e. 4), the stator iron of the 18-stator-slot FRPMM is less likely to saturate than the others.

E. Influence of Stator Pole Shoe/Airgap and PM Thickness/ Airgap on Power Factor

Since the power factor of FRPMM tends to be low, and the power factor is greatly affected by the airgap structural parameters, the influences of stator inner diameter/airgap D_i/g and PM radial thickness/airgap h_m/g on the power factor are investigated in this part. Fig. 7 and 8 present the variations of power factor with D_i/g and h_m/g, respectively. It can be seen that the power factor increases continuously with D_i/g. This is because when the stator inner diameter D_i increases, the slot area decreases and the winding turns per phase is reduced. Therefore, the winding inductance and synchronous inductance decrease. As the power factor is derived as:

$$PF = 1\Big/\sqrt{1+\left(\frac{L_s I_s}{\psi_m}\right)^2} \tag{18}$$

where I_s is the stator current, ψ_m is the PM flux linkage and L_s is the synchronous inductance. As L_s is reduced, the power factor increases. In Fig. 8, it is found that the power factor initially increases with h_m/g, but then the power factor decreases. When h_m gets bigger, the PM flux linkage ψ_m in Eqn. 18 becomes higher, and thus the power factor increases. However, the effective airgap length also increases with h_m, and hence the synchronous inductances gets larger and power factor gets smaller. Therefore, there is a maximal power factor when h_m/g varies.

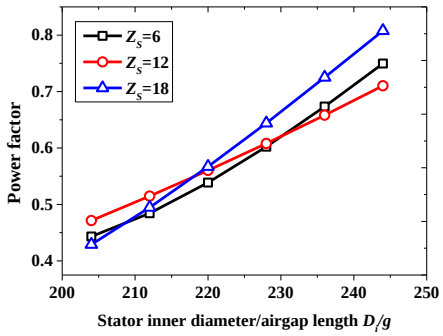

Fig. 7. Effect of stator inner diameter/airgap length on power factor.

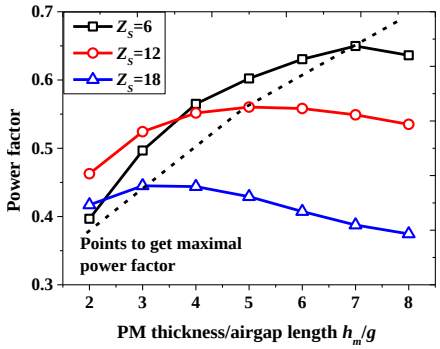

Fig. 8. Effect of PM thickness/airgap length on power factor.

IV. Geometric Design of Stator and Rotor

A. Stator Geometry

The flux per stator winding pole under no load condition can be given as:

$$\phi_m = 2\lambda_w l_{stk} B_m / \pi \tag{19}$$

where λ_w is the winding pitch. If full-pitch windings are assumed, the winding pitch can be expressed as:

$$\lambda_w = 2\pi r_g / 2P \tag{20}$$

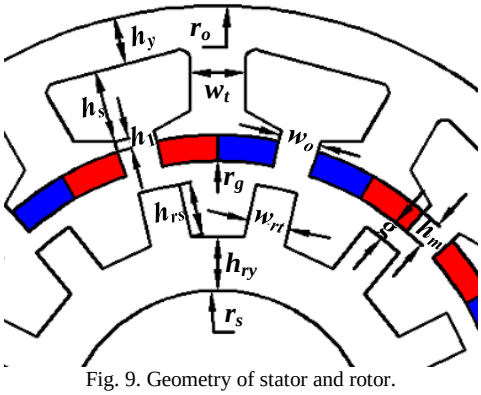

Fig. 9. Geometry of stator and rotor.

Then, the flux per stator winding pole ϕ_m in Eqn. 19 can be rewritten as:

$$\phi_m = 2 r_g l_{stk} B_m / P \tag{21}$$

If the flux density of stator yoke is set as B_y, the thickness of stator yoke will be derived as:

$$h_y = \frac{\phi_m}{2 B_y k_{stk} l_{stk}} = \frac{r_g B_m}{P B_y k_{stk}} \tag{22}$$

Similarly, if the flux density of stator teeth is assumed to be B_t, the tooth width can be obtained as:

$$w_t = \frac{\phi_m}{3SPPk_{stk} l_{stk} B_t} = \frac{4 r_g B_m}{Z_s k_{stk} B_t} \tag{23}$$

Moreover, in order to maximize the torque density as well as reduce the risk of PM demagnetization, the PM thickness is usually chosen as:

$$h_m = 4g \sim 6g \tag{24}$$

where g is the airgap length. Since the torque density reaches the maximal value when the slot opening ratio is around 0.25 [3], the slot opening width w_o can be given as:

$$w_o = \pi \left(r_g + h_m \right) / 2Z_s \tag{25}$$

On the one hand, the total slot area of a FRPMM A_{slot} can be expressed based on the winding electric loading A_e and the current density J_e as:

$$A_{slot} = 2\pi \left(r_g + h_m \right) A_e / J_e S_{fg} \tag{26}$$

where S_{fg} is the slot fill factor. Meanwhile, the slot area A_{slot} can be calculated using the stator geometric parameters:

$$A_{slot} = \pi \left(r_g + h_m + h_1 + h_s \right)^2 - \pi \left(r_g + h_m + h_1 \right)^2 - Z_s w_t h_s \tag{27}$$

Combining the Eqns. 26 and 27, the slot depth h_s can be determined. Then, the stator outer radius r_o can be given as:

$$r_o = r_g + h_m + h_1 + h_s + h_y \tag{28}$$

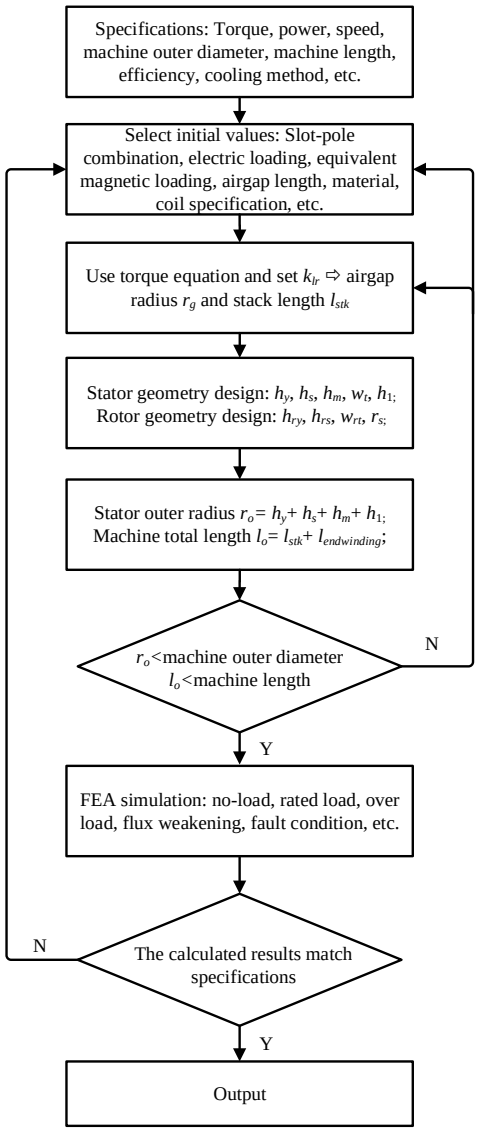

Fig. 10. Design flow of FRPMM.

B. Rotor Geometry

When the flux density of rotor yoke and teeth are set as B_{ry}, and B_{rt}, respectively, the rotor yoke thickness h_{ry} and rotor teeth width w_{rt} can be obtained on the analogy of Eqns. 22 and 23. As the rotor pole pair number is Z_r, the h_{ry} and w_{rt} are derived as:

$$h_{ry} = r_g B_m / Z_r B_{ry} k_{stk} \tag{29}$$

$$w_{rt} = 4r_g B_m / Z_r k_{stk} B_{rt} \quad (30)$$

Then, the rotor slot depth h_{rs} is determined as:

$$h_{rs} = r_s + h_{ry} \quad (31)$$

V. Design Methodology and Evaluations

A. Design Procedure

Based on the analytical equations derived in the former part, the design method to of a FRPMM would be realized through the following procedure (as illustrated in Fig. 10):

1) Based on the investigations in Figs. 3 to 7, the initial values including slot-pole combination, electric loading, equivalent magnetic loading, etc. can be selected.

2) The airgap radius r_g and the stack length l_{stk} will be obtained using Eqns. 16 and 17.

3) With the employment of Eqns. 19 to 31, the detailed stator and rotor geometry can be determined.

4) Check if the machine geometric parameters satisfy the design specifications. If so, proceed to the FEA verifications at different operation conditions. If not, reset the initial values.

5) By FEA simulations, the electromagnetic performances such as flux density, back-EMF, torque, pulsating torque, etc. can be achieved. Make sure whether all the performances match the design requirements. If not, adjust the design parameters and iterate the design flow until everything is appropriate.

6) Finally, it is the result output.

B. Case Study

TABLE III
SPECIFICATIONS OF A FRPMM

Parameter	Value	Parameter	Value
Rated torque	8 Nm	Stator outer diameter	130mm
Rated speed	300 rpm	Rotor inner diameter	32mm
Rated power	0.25 kW	Stack length	120mm
Airgap length	0.6mm	Cooling method	Natural cooling
PM material	N38SH	Iron material	50WW470

TABLE IV
DESIGN PARAMETERS OF THE FRPMM

	Parameter	Value	Parameter	Value
Stator	Outer diameter	124mm	Inner diameter	79mm
	Slot number	12	Winding pole pair	1
	Teeth width	11.5mm	Teeth flux density	1.1T
	Slot depth	13.5mm	Yoke flux density	1.0T
	Yoke thickness	6mm	Turns per phase	300
Magnet	Magnet width	7.8mm	PM thickness	3mm
Rotor	Outer diameter	77.8mm	Inner diameter	32mm
	Slot depth	10.4mm	Slot number	17
	Yoke thickness	12.5mm	Yoke flux density	1.0T
	Teeth width	4mm	Teeth flux density	1.2T

TABLE V
RESULTS COMPARISON OF THE DESIGN METHOD AND FEA

Parameter	Analytical design method	FEA
Torque	8.4Nm	7.97Nm
Back-EMF	44.8V	42.4V
PM flux linkage	1.43 Wb	1.35 Wb

The specification of the FRPMM is shown in Table III. For a considerable margin, the rated torque is set to be 105% of the rated torque, i.e. 8.4 Nm. The first step is to choose the slot-pole combination. The 12-stator-slot/17-rotor-slot combination is selected mainly because of its relatively high average torque and low pulsating torque (including cogging torque and ripple torque). After that, using analysis result in Fig. 7, the electric loading and equivalent magnetic loading are chosen. Next, based on the torque equation in Eqn. 14, the airgap radius can be determined. Then, after selecting the appropriate flux density values of stator tooth, stator yoke, rotor tooth and rotor yoke, the detailed structural parameters of stator and rotor are made clear. Finally, the machine dimensions and magnetic parameters are summarized in Table IV. Moreover, to validate the machine design parameters, the analytical design model is simulated using FEA. It can be found in Table V that the FEA and analytical results have shown good correlations. Thus, a conclusion can be drawn that the proposed analytical design method is effective and applicable.

C. Experimental Study

(a) (b)

Fig. 11. 12-slot/17-pole FRPMM prototype: (a) Stator; (b) Rotor.

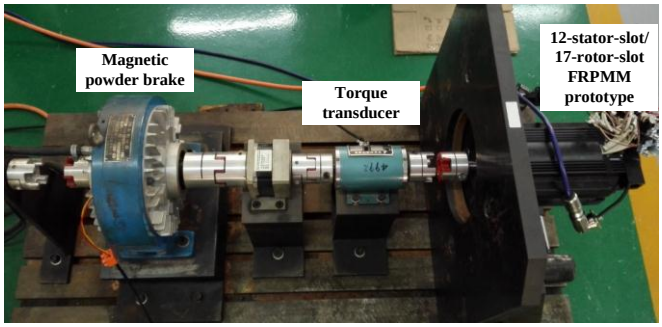

Fig. 12. Test bed of the FRPMM prototype.

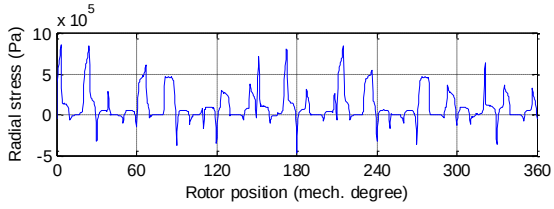

(a)

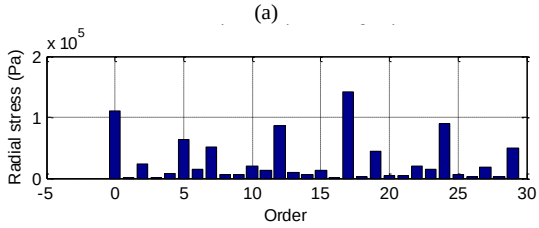

(b)

Fig. 13. Radial stress analysis of the FRPMMs prototype.

To verify the calculated results by the analytical method and FEA, the FRPMM prototype has been built. Its major parameters are listed in Table IV. The structure and test bed of the prototype are shown in Figs. 11 and 12, respectively. Since the unbalanced radial force in the 17-rotor-slot FRPMM

prototype is negligible, it has not been considered. The explanation is as follows. According to [33], only the first spatial order component of the radial stress has contributions to the unbalanced magnetic force. In Fig. 13, it can be seen that the first order components of the radial stress in the FRPMM prototype is very small. Hence, the 17-rotor-slot FRPMM is suitable.

Fig. 14 shows the phase back-EMF waveform at 300rpm, and the back-EMF predicted by FEA is compared with the measurements. The total harmonic distortion (THD) of FEA and experiments are 1.26% and 2.63%, respectively. So the back-EMF waveforms are quite sinusoidal. After that, the variations of average torque with the phase current calculated by FEA and the proposed analytical method are compared to that of the experiments in Fig. 15. The blue triangle represents the analytical design value. It can be found that the calculated results match well with those measured ones. The maximal current is chosen as 4A. The explanation is as follows. The insulation class of the prototype is set as F level, and the working temperature is around 120 centigrade. The PM material is selected as N38SH, and its demagnetization flux density is 0.5 T. When the phase current is 7A, the PM will demagnetize, as shown in Fig. 16. So the maximal current when doing the experiment is set as 60% (4 A) for a considerable design margin. Finally, Table VI compares the electromagnetic performances by FEA and experiments. Thus, the feasibility of the proposed analytical design method can be seen.

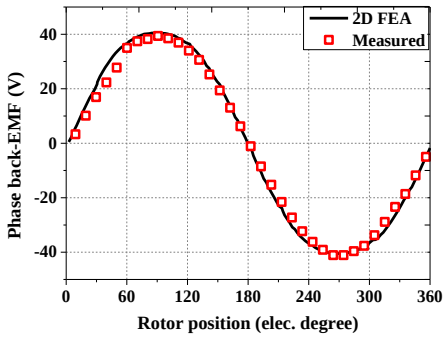

(a)

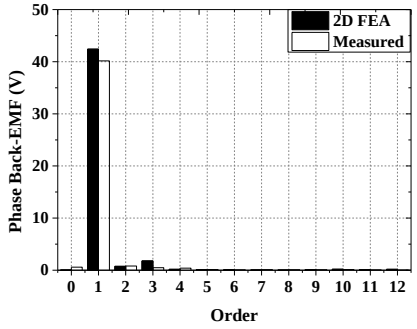

(b)

Fig. 14. Back-EMF waveforms at rated speed 300rpm: (a) Waveform; (b) FFT analysis.

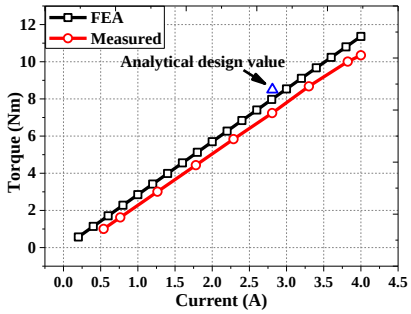

Fig. 15. Output torque vs phase current.

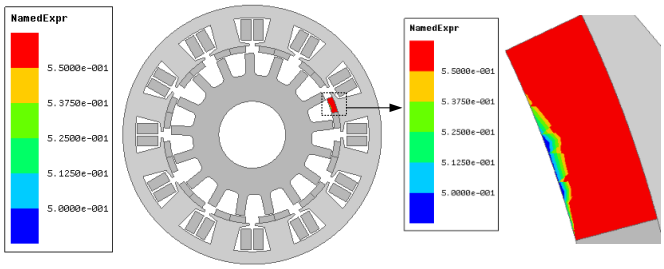

Fig. 16. Demagnetization of the FRM prototype.

TABLE VI
PERFORMANCES OF THE FRPMM PROTOTYPE

Parameter	FEA	Experiment
Phase back-EMF magnitude at 300rpm	42.4V	41.2V
THD of the phase back-EMF at 300 rpm	1.26%	2.63%
Average torque at rated current	7.97Nm	7.24Nm
Power factor	0.756	0.746
Total losses	99.5W	116.7W
Efficiency	60.3%	57.3%
Torque per weight	0.66Nm/kg	0.60Nm/kg

VI. CONCLUSION

In this paper, an analytical design methodology of three-phase FRPMM is proposed, which includes the sizing equation, geometric design of stator and rotor, feasible slot-pole combinations and the recommended winding configurations of each combination. Moreover, to help to select the initial design values, the effects of some key parameters in the sizing equation such as number of stator and rotor slots, airgap radius, electrical loading and equivalent magnetic loading are investigated based on FEA. It is found that when the rotor radius is around 100mm, the optimized rotor slot number for 6-stator-slot, 12-stator-slot and 18-stator-slot FRPMMs with non-overlapping windings are 8, 14 and 21, respectively. However, it should be noted that the optimal rotor slot number for a maximum torque is not a constant but changes with the machine outer diameter. The larger the diameter, the more the optimal rotor slots. Finally, through comparisons among the experimental results, the analytical design value and FEA, the effectiveness of the proposed design methodology can be seen.

REFERENCES

[1] R. Deodhar, S. Andersson, I. Boldea, and T. Miller, "The flux-reversal machine: A new brushless doubly-salient permanent-magnet machine," *IEEE Trans. Ind. Appl.*, vol. 33, no. 4, pp. 925–934, Jul. 1997.

[2] C. Wang, S. Nasar, etc., "Three phase flux reversal machine (FRM)," *IEE Proc.-Electr. Power Appl.*, vol. 146, no. 2, pp. 139–146, Mar. 1999.

[3] Y. Gao, R. Qu, D. Li, etc., "Design of three-phase flux reversal machines with fractional-slot windings," *IEEE Trans. Ind. Appl.*, vol. 52, no.4, pp. 2856-2864, Jul./Aug. 2016.
[4] C. X. Wang, I. Boldea and S. A. Nasar, "Characterization of three phase flux reversal machine as automotive generator," *IEEE Trans. Energy Convers.*, vol. 16, no. 1, pp. 74-80, Mar. 2001.
[5] I. Boldea, L. N. Tutelea, L. Parsa and D. Dorrell, "Automotive electric propulsion systems with reduced or no permanent magnets: an overview," *IEEE Trans. Ind. Electro.*, vol. 61, no. 10, pp. 5696-5711, Oct. 2014.
[6] I. Boldea, L. Zhang, and S. A. Nasar, "Theoretical characterization of flux reversal machine in low-speed servo drives-the pole-PM configuration," *IEEE Trans. Ind. Appl.*, vol. 38, no. 6, pp. 1549–1557, Nov./Dec. 2002.
[7] D. S. More and B. G. Fernandes, "Analysis of flux-reversal machine based on fictitious electrical gear," *IEEE Trans. Energy Convers.*, vol, 25, no. 4, pp. 940-947, Dec. 2010.
[8] D. S. More, H. Kalluru, and B. G. Fernandes, "Comparative analysis of flux reversal machine with fractional slot concentrated winding PMSM," in *Proc. IEEE Ind. Electron. Conf.*, Nov. 2008, pp. 1131–1136.
[9] J. Zhang, M. Cheng, Z. Chen, and W. Hua, "Comparison of stator mounted permanent magnet machines based on a general power equation," *IEEE Trans. Energy Convers*., vol. 24, no. 4, pp. 826–834, Dec. 2009.
[10] Y. Gao, R. Qu, D. Li, etc., "Consequent-pole flux-reversal permanent-magnet machine for electric vehicle propulsion," *IEEE Trans. Appl. Supercond*., vol. 26, no. 4, p. 5200105, Jun. 2016.
[11] Z. Zhu, Z. Wu, etc., "Novel electrical machines having separate PM excitation stator," *IEEE Trans. Magn*., vol. 51, no. 4, p. 8104109, 2014.
[12] Z. Z. Wu and Z. Q. Zhu, "Partitioned stator flux reversal machine with consequent-pole PM stator," *IEEE Trans. Energy Convers*., vol. 30, no. 4, pp. 1472-1482, Dec. 2015.
[13] M. Zheng, Z. Wu, Z. Zhu, "Partitioned stator flux reversal machines having Halbach array PMs," in *Proc. 2015 IEEE Magn. Conf. (Intermag)*, Beijing, China, 2015.
[14] Z. Z. Wu and Z. Q. Zhu, "Comparative analysis of partitioned stator flux reversal PM machines having fractional-slot nonoverlapping and integer-slot overlapping windings," *IEEE Trans. Energy Convers*., vol. 31, no. 2, pp. 776-788, Jun. 2016.
[15] D. More and B. Fernandes, "Power density improvement of three phase flux reversal machine with distributed winding," *IET J. Electr. Power Appl*., vol. 4, no. 2, pp. 109–120, Feb. 2010.
[16] Y. S. Kim, T. H. Kim, Y. T. Kim, W. S. Oh and J. Lee, "Various design techniques to reduce cogging torque in flux-reversal machines," in *Proc. Eighth Int. Conf. Electr. Mach. Syst. (ICEMS)*, vol. 1, pp.261–263, 2005.
[17] T. Kim, S. Won, K. Bong and J. Lee, "Reduction in cogging torque in flux reversal machine by rotor teeth pairing," *IEEE Trans. Magn.*,vol. 41, no. 10, pp. 3964–3966, Oct. 2005.
[18] C. Sikder, etc., "Cogging torque reduction in flux-switching permanent-magnet machines by rotor pole shaping," *IEEE Trans. Ind. Appl.* vol. 51, no. 5, pp. 3609-3619, Sept./Oct. 2015.
[19] L. Hao, etc., "Cogging torque reduction of axial-field flux-switching permanent magnet machine by rotor tooth notching," *IEEE Trans. Magn*., vol. 51, no. 11, Nov. 2015.
[20] D. Xu, M. Lin, X. Fu, etc., "Cogging torque reduction of a hybrid axial field flux-switching permanent magnet machine with three-methods," *IEEE Trans. Appl. Supercond*., vol. 26, no. 4, p.5201305, Jun. 2016.
[21] D. S. More and B. G. Fernandes, "Analysis of flux-reversal machine based on fictitious electrical gear," *IEEE Trans. Energy Convers.*, vol, 25, no. 4, pp. 940-947, Dec. 2010.
[22] D. S. More, H. Kalluru, etc, "d-q equivalent circuit representation of three-phase flux reversal machine with full pitch winding," in *Proc. IEEE Power Electron. Spec. Conf.*, 2008, pp. 1208–1214.
[23] D. S. More and B. G. Fernandes, "Modelling and performance of three phase 6/14 pole flux reversal machine," *IET Elect. Power Appl.*, vol. 7, no. 2, pp. 131–139, Feb. 2013.
[24] Z. Zhu and D. Evans, "Overview of recent advances in innovative electrical machines, with particular reference to magnetically geared switched flux machines," Keynote Speech, *Int. Conf. Electrical Machines and Systems* (ICEMS2014), Hangzhou, China, 2014, pp. 1-10.
[25] R. Qu, D. Li and J. Wang, "Relationship between magnetic gears and vernier machines," in *Proc. Int. Conf. Electr. Mach. Syst.* (ICEMS), Beijing, China, 2011, pp. 1-6.
[26] D. Li, R. Qu, J. Li, "Topologies and analysis of flux-modulation machines," in *Proc. Energy Convers. Congr. and Expo*. (ECCE), pp. 2153-2160, 2015.
[27] D. Li, R. Qu, J. Li, etc., "Synthesis of flux switching permanent magnet machines", *IEEE Trans. Energy Conv*., vol. 31, no. 1, pp. 106-117, 2016.
[28] I. Boldea, C. X. Wang, and S. A. Nasar, "Design of a three-phase flux reversal machine," *Elect. Mach. Power Syst.*, vol. 27, pp. 849–863, 1999.
[29] Y. Gao, R. Qu, D. Li, etc., "Torque performance analysis of three-phase flux reversal machines for electric vehicle propulsion," in *Proc. 2016 IEEE Transportation Electrification Conference and Expo, Asia-Pacific (ITEC Asia-Pacific)*, vol. 1, pp. 296-301, Jun. 2016.
[30] T. H. Kim and J. Lee, "A study of the design for the flux reversal machine," *IEEE Trans. Magn*., vol. 40, no. 4, pp. 2053–2055, Jul. 2004.
[31] Y. Gao, R. Qu, D. Li, J. Li, "Design procedure of flux reversal permanent magnet machines", in *Proc. International Conference on Electrical Machines (ICEM)*, Lausanne, Switzerland, 2016.
[32] Z. Q. Zhu, and D. Howe, "Instantaneous magnetic-field distribution in brushless permanent-magnet dc motors, part III effect of stator slotting," *IEEE Trans. Magn*., vol. 29, no. 1, pp. 143-151, Jan. 1993.
[33] Z. Q. Zhu, M. Jamil, and L. Wu, "Influence of slot and pole number combinations on unbalanced magnetic force in PM machines with diametrically asymmetric windings," *IEEE Trans. Ind. Appl.*, vol. 49, no. 1, pp. 19–30, Jan./Feb., 2013.